

Active Disturbance Rejection Control of a MEMS Gyroscope

Brian Fast^{*}, Robert Miklosovic[†], Aaron Radke[‡]

Abstract— A novel method is proposed for controlling the position of a vibrating proof mass in a z-axis MEMS gyroscope while simultaneously approximating its rotation rate in a third dimension independent of cross coupling terms. Designing the controller to require minimal model information and reject a broad range of disturbances, including the cross coupling terms, dramatically reduces controller complexity over a broader range of applications. A multi sensor solution is also presented for approximating the rotation rate. The proposed method is demonstrated in a simulation of a z-Axis MEMS gyroscope developed by the University of California-Berkeley.

Keywords— MEMS Gyroscope, rotation rate sensing, active disturbance rejection control, extended state observer.

I. INTRODUCTION

Sensing the rotation rate around a specific axis in a micro-electrical-mechanical system (MEMS) sized device adds significant value because a system's inertial information can be used for improving stability, image stabilization, and directional navigation [1]. In general, MEMS applications are valuable due to their size. As mobile and autonomous devices continue to incorporate more intelligence to interact with the world, the gyroscope is quickly becoming a key sensor [1-9].

Approximating the rotation rate within a MEMS gyroscope is nontrivial. The sensing is based on oscillating a proof mass at a resonant frequency along the drive axis while holding the sense axis stationary. When a rotation rate is applied to the z-axis, Coriolis acceleration is imposed orthogonal to the oscillation of the proof mass [5]. An approximation of the rotation rate is obtained from the control effort required to force the mass to remain stationary.

The accuracy of rate sensing is typically dependent on control system performance. Specifically, variations in cross coupling terms due to fabrication imperfections on a microscopic level and environmental variations make controlling position of the proof mass difficult due to its nonlinear time-varying nature. Most solutions assume zero cross coupled damping forces, but allow a frequency mismatch [2-4] while other methods try to control only one axis. Some techniques attempt to improve rotation rate approximation by adaptively identifying cross coupling term coefficients but with suboptimal performance [5-9].

This paper proposes an active disturbance rejection control (ADRC) solution [10-12] that compensates for unknown cross coupling terms while controlling the position of the vibrating proof mass in two dimensions. The drive

axis is forced to track a sinusoidal input while the sense axis is kept stationary. A method is also presented for measuring the rotation rate using part of the sense axis control signal. The solution requires two sensors for continuously approximating the rotation rate, however, the additional hardware complexity is offset by simplifying calibration thus design complexity. Variations within any given operating environment typically have a significant impact on sensor performance and frequent calibration is often required. Identifying individual parameters of a system is challenging even under lab conditions. As a result, a simplified calibration method is used to identify system dynamics with a single measurement over a finite period of time. The calibrated signal is used to extract rotation rate dependent dynamics. The robustness of this method is based on the ability to quickly and simply recalibrate the system in the operational environment. The calibration is performed when the sensor is intentionally held or is known to be stationary, for a short period of time, and a new calibration signal is obtained.

This unified approach reduces the design process and increases robustness. The paper is organized as follows. In Section II, a new control method is proposed. Section III presents a unique method of estimating the rotation rate. Simulation results are given in Section IV. Section V provides concluding remarks.

II. DISTURBANCE REJECTION CONTROL METHOD

The mechanical model of a z-axis MEMS gyroscope is a mass-spring-damper system as shown in Figure 1.

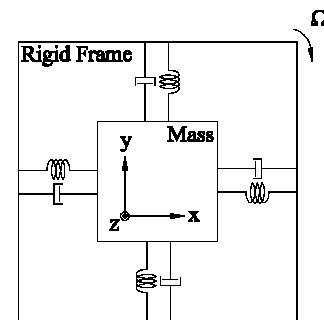


Figure 1: Mechanical model of a z-axis MEMS gyroscope

Equations governing the z-axis [1-9] are given as

$$\ddot{x} + 2\zeta\omega_n\dot{x} + \omega_n^2x + \omega_{xy}y - 2\Omega\dot{y} = \frac{k}{m}u_d(t) \quad (1)$$

and

$$\ddot{y} + 2\zeta_y\omega_y\dot{y} + \omega_y^2y + \omega_{xy}x + 2\Omega\dot{x} = \frac{k}{m}u_s(t) \quad (2)$$

^{*}Brian Fast, Northrop Grumman, CA (bfast@ieee.org)

[†]Robert Miklosovic, Rockwell Automation, OH (rmiklosovic@ieee.org)

[‡]Aaron Radke, Lockheed Martin, OH (radke@ieee.org)

where x and y are the drive and sense axis position, respectively, ω_n and ω_y are dependent on each axes natural frequency, $u_d(t)$ and $u_s(t)$ are the drive and sense axis control inputs, m is the mass of the vibrating element or proof mass, and the gain k includes sensor, actuator, and amplifier gains. Coriolis acceleration is defined by $2\Omega\dot{x}$ and $2\Omega\dot{y}$, where Ω is an unknown time-varying rotation rate. The compliant coupling between the two axes is represented by $\omega_{xy}y$ and $\omega_{yx}x$.

To demonstrate how ADRC is applied to control position of the proof mass, an example is given for the drive axis with the understanding that the sense axis uses a similar controller. First, (1) is rewritten as

$$\ddot{x} = f_d(x, \dot{x}, y, \dot{y}, w) + \frac{k}{m}u_d(t) \quad (3)$$

where $f_d(x, \dot{x}, y, \dot{y}, w)$, denoted as f_d , incorporates internal dynamics as well as any external disturbance w . A state space model is constructed

$$\begin{aligned} \dot{\phi} &= A\phi + Bu_d + Ef_d \\ x &= C\phi \end{aligned} \quad (4)$$

$$A = \begin{bmatrix} 0 & 1 & 0 \\ 0 & 0 & 1 \\ 0 & 0 & 0 \end{bmatrix}, B = \begin{bmatrix} 0 \\ k/m \\ 0 \end{bmatrix}, E = \begin{bmatrix} 0 \\ 0 \\ 1 \end{bmatrix}, C = \begin{bmatrix} 1 \\ 0 \\ 0 \end{bmatrix}^T$$

where $\phi = [\phi_1, \phi_2, \phi_3]^T = [x, \dot{x}, f_d]^T$ includes an extended state to estimate f_d . An observer is then created to estimate the states.

$$\dot{\hat{\phi}} = A\hat{\phi} + Bu + L(x - C\hat{\phi}) \quad (5)$$

The observer's characteristic equation is set equal to a desired polynomial $\lambda_o(s) = |sI - A + LC| = (s + \omega_o)^3$ and the observer gain L is determined as a function of a single parameter.

$$L = [3\omega_o, 3\omega_o^2, \omega_o^3]^T \quad (6)$$

A disturbance rejection control law

$$u_d = (u_0 - \hat{\phi}_3)m/k \quad (7)$$

is applied in (3) to cancel f_d and reduce the plant to a double integrator at low frequencies.

$$\ddot{x} = (f_d - \hat{\phi}_3) + u_0 \approx u_0 \quad (8)$$

Note that m/k is the inverse of the system's high frequency gain and is typically determined empirically. A tracking control law with reference r is applied. It consists of a PD controller with acceleration feed forward.

$$u_0 = k_p(r - \hat{\phi}_1) + k_d(\dot{r} - \hat{\phi}_2) + \ddot{r} \quad (9)$$

With the assumption that $\ddot{x} \approx u_0$, the characteristic equation of the closed loop system is set equal to a desired polynomial

$\lambda_c(s) = (s^2 + k_d s + k_p) = (s + \omega_c)^2$ and the controller gains are determined as a function of a single parameter.

$$[k_p, k_d] = [\omega_c^2, 2\omega_c] \quad (10)$$

III. ROTATION RATE ESTIMATION

Once the sense axis position is accurately controlled, the rotation rate can be estimated. This section exploits the unique formulation of ADRC to extract the rotation rate from the disturbance estimation in the sense axis control law.

A. Formulation

Extracting rotation rate from the control law is based on a stored calibration that is obtained when the device is initially at rest. Then when the device is operational, rotation rate is approximated by subtracting the calibrated signal from the sense axis control signal and scaling it.

Rotation rate is extracted from the estimation of f_s by representing the sense axis disturbance rejection control law similar to that of the drive axis in (7)

$$u_s = (u_0 - \hat{f}_s)m/k \quad (11)$$

where

$$f_s = -2\zeta_y \omega_y \dot{y} - \omega_y^2 y - \omega_{xy} x - 2\Omega \dot{x}. \quad (12)$$

The separation first requires an initial run to calibrate the sense control signal while the MEMS gyroscope remains stationary.

$$u_{s_cal} = (u_0 - \hat{f}_{s_cal})m/k \quad (13)$$

Since the calibrated control signal produces dynamic information not associated with the rotation rate when it is stationary

$$f_{s_cal} = -2\zeta_y \omega_y \dot{y} - \omega_y^2 y - \omega_{xy} x, \quad (14)$$

the calibrated control signal is subtracted from the sense control signal yields

$$u_s - u_{s_cal} = 2\Omega \dot{x} \frac{m}{k}. \quad (15)$$

As a result, rotation rate is estimated by

$$\hat{\Omega} = \frac{(u_s - u_{s_cal})k}{2\dot{x}m}. \quad (16)$$

Clearly if \dot{x} is equal to zero then (16) will be undefined. However the control objective causes \dot{x} to be a known sinusoid at the resonant frequency of the system. With this knowledge the calibrated signal is constructed to avoid this condition by collecting data slightly before and after this discontinuity.

The accuracy of this rate approximation is independent of an accurate model, specifically the cross coupling terms. Explicit knowledge of the system states and coefficients in

(12) and (14) is unnecessary because they are accounted for in the estimate of f_s .

B. Calibration Issues

In this scheme, approximating the rotation rate from a single sensor creates discontinuities due to a finite set of calibrated data. By combining the results from two gyroscopes, and staggering the calibration reset, a continuous approximation of the rotation rate is generated. A theoretical example of the two sensor scheme is shown in Figure 2.

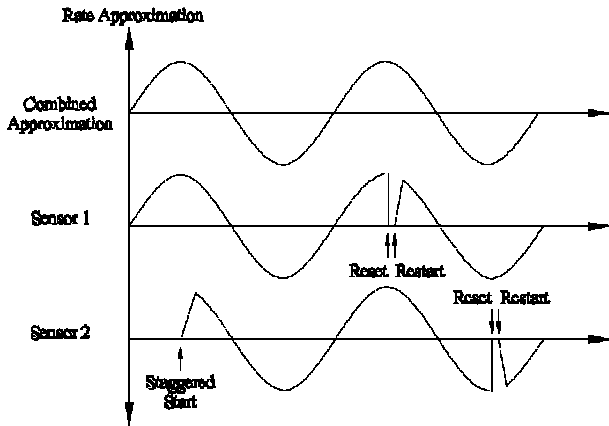


Figure 2: Staggering of Rate Approximation Using 2 MEMS Gyroscopes

The two sensor scheme generates good results when the rate approximation from one sensor quickly converges to the desired rotation rate. For this example, the convergence is shown in Figure 3, and takes place in approximately 100 μ s.

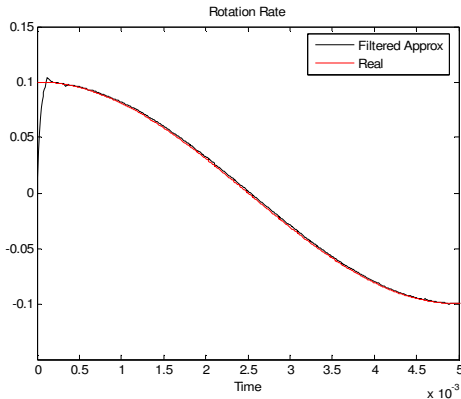


Figure 3: Rate Approximation with a Non Zero Initial Condition

IV. SIMULATION RESULTS

The proposed solutions are simulated on a model of the z-axis MEMS gyroscope developed by the University of California Berkeley [6]. The plant parameters used in the simulation are as follows:

$$\begin{aligned} \omega &= 84194.7 \text{ rad / s} \\ \omega_n &= 81681.4 \text{ rad / s} \\ \omega_y &= 80684.6 \text{ rad / s} \\ \omega_{xy} &= 14856 \text{ rad / s} \\ \zeta &= 4.5455 \times 10^{-5} \\ \zeta_y &= 3.125 \times 10^{-4} \\ m &= 2 \times 10^{-9} \text{ kg} \\ A &= 50 \\ k &= 0.8338 \end{aligned}$$

For the drive and sense axes, the power spectrum density (PSD) of the input noise is 5.095×10^{-24} , and the output noise PSD is 1.49×10^{-27} . The control signals saturation is 100mV, and the controller parameters are

$$\omega_c = 500000, \quad \omega_o = 2500000, \quad k/m = 4.856 \times 10^8$$

The controller gains ω_c and ω_o are chosen by monitoring the output of the system compared to the reference while maintaining a minimum 6dB of gain margin and 30° of phase margin. The high frequency gain k/m is chosen by examining the frequency response of the system. It is equal to the low frequency gain multiplied by the squared angular velocity at the peak of the resonance.

The approximated rotation rate of a fast time varying signal, passed through a low pass filter, is shown in Figure 4. For this example, the actual rotation rate is equal to a sinusoid with amplitude of 0.1 at a frequency of 100 Hz. The error between the approximated and the actual rotation rate is also shown in Figure 5.

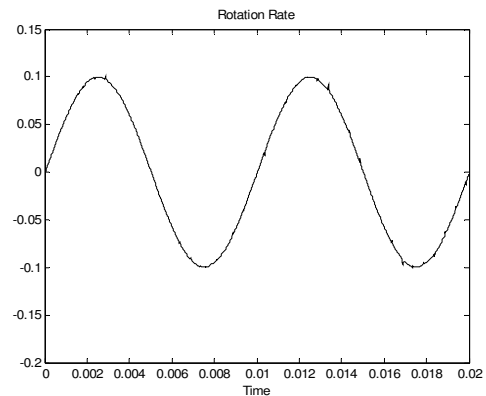


Figure 4: Filtered Approximated Rotation Rate with Noise

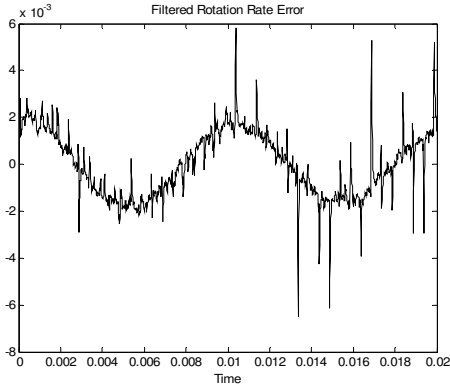


Figure 5: Approximated Rotation Rate Error with Noise

The peak error, for this example, is about two percent. Most of the error is contributed to the phase delay of the low pass filter. The ability to approximate a less structured signal, demonstrates the robustness of the solution, and these results are shown in Figure 6.

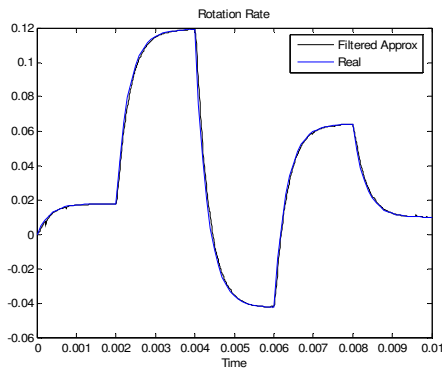


Figure 6: Filtered and Real Rotation Rate

The remaining figures provide information concerning the state of the system. Figure 7 shows the position of the drive axis driven to 50 μ m at a resonant frequency of 12,740Hz and Figure 8 is a magnified view of the drive axis position.

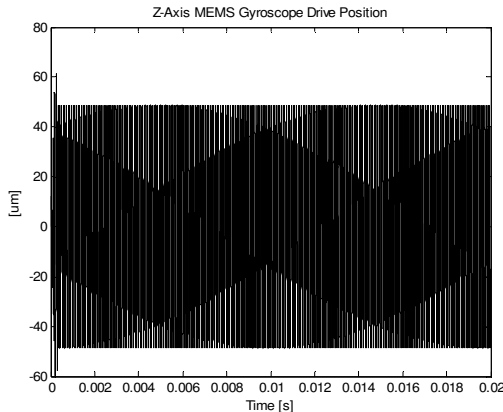


Figure 7: Actual Drive Position Controlled

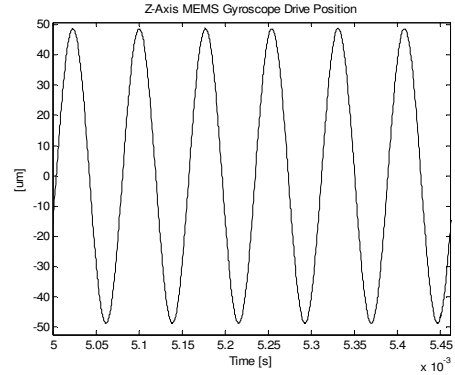


Figure 8: Actual Drive Position Controlled Magnified

Figure 9 shows the position of the sense axis, while the system is being controlled, and the desired position is equal to zero.

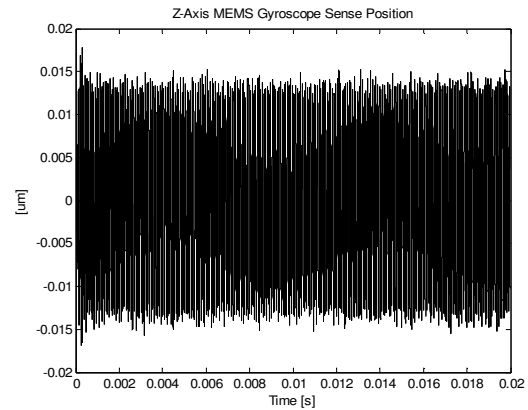


Figure 9: Actual Sense Position Controlled

Figure 10 shows the open loop frequency response, for a measure of robustness, where the gain margin is 10.9dB and the phase margin is 31.7°. The systems resonance is not removed to minimize the control effort when the system is driven at its resonant frequency.

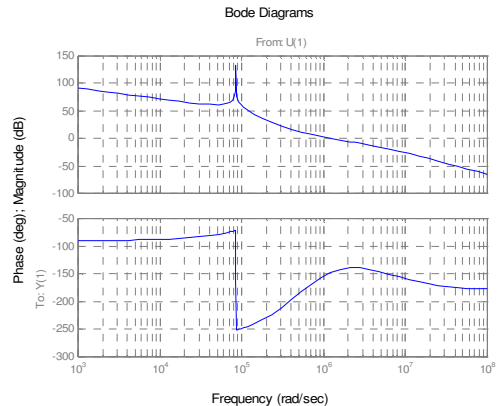


Figure 10: Open Loop Frequency Response

V. CONCLUDING REMARKS

Simulation results suggest that active disturbance rejection control can be applied in a straightforward manner to accurately control the position of a vibrating proof mass. The unique control law removes the need for accurate model information. Furthermore, a method for approximating the time varying rotation rate is also extracted from it. The solution appears to be robust with respect to environmental variations.

REFERENCES

- [1] A.M. Shkel, R. Horowitz, Ashwin A. Seshia, Sungsu Park, and Roger T. Howe, "Dynamics and control of micromachined gyroscopes," Proceedings of American Control Conference, pp. 2119-2124, 1999.
- [2] R. T. M'Closkey, A. Vakakis, "Analysis of a micromsensor automatic gain control loop," Proceedings of American Control Conference, pp. 3307-3311, 1999.
- [3] R. Leland, "Adaptive mode tuning for vibrational gyroscopes," IEEE Transactions on Control Systems Technology, Vol. 11, No. 2, pp. 242-247, 2003.
- [4] R. Leland, Y. Lipkin, and A. Highsmith, "Adaptive oscillator control for a vibrational gyroscope," Proceedings of American Control Conference, pp. 3347-3352, 2003.
- [5] L. Dong and R.P. Leland, "The adaptive control system of a MEMS gyroscope with time-varying rotation rate," IEEE Proceedings of American Control Conference, pp. 3592-3597, June 2005.
- [6] S. Park, "Adaptive control strategies for MEMS gyroscopes," PhD Dissertation, The University of California Berkely, 2000.
- [7] S. Park, R. Horowitz, "Adaptive control for z-axis MEMS gyroscopes," Proceedings of American Control Conference, pp. 1223-1228, 2001.
- [8] R. Leland, "Lyapunov based adaptive control of a MEMS gyroscope," *proceedings of American Control Conference*, pp.3765-3770, 2002.
- [9] S. Park, R. Horowitz, "Adaptive control for the conventional mode of operation of MEMS gyroscopes," Journal of Microelectromechanical Systems, Vol. 12, No. 1, pp. 101-108, Feb. 2003.
- [10] J. Han, "Nonlinear design methods for control systems", Proc. 14th IFAC World Congress, 1999.
- [11] Z. Gao, "Scaling and parameterization based controller tuning," Proceeding of American Control Conference, pp. 4989-4996, 2003.
- [12] A. Radke and Z. Gao, "A survey of state and disturbance observers for practitioners," in *Proc. of the American Control Conference ACC/IEEE*, Minneapolis, Minnesota, June 14-16, 2006.